Geotechnical Engineering Journal of the SEAGS & AGSSEA Vol. 45 No.3 September 2014 ISSN 0046-5828

Centrifuge Modelling of Improved Ground

M. Kitazume[1], Y. Morikawa[2] and S. Nishimura[3]
[1]Department of Civil and Environment Engineering, Tokyo Institute of Technology, Tokyo, Japan
[2]Geotechnical Engineering Field, Port and Airport Research Institute, Japan
[3]Faculty of Engineering, Hokkaido University, Japan
E-mail: kitazume@cv.titech.ac.jp

ABSTRACT: Soft soil is often encountered during infrastructure construction, in which large ground settlement and stability failure can be anticipated. There are many soil improvement techniques in existence to counter these problems. The behaviour of improved ground is affected by many factors such as the physical and mechanical properties of the original ground and the improved ground, interaction of the original and improved ground, external loading conditions, *etc*. Many centrifuge model tests have been carried out on the topic of ground improvement, which can be classified into two categories: the investigation of soil properties' changes and the behavior of original ground during ground improvement work or the investigation of the behavior of improved ground. The Port and Airport Research Institute carried out many centrifuge model tests on research topics related to several ground improvement techniques over many years. In this report, several examples of centrifuge modelling carried out at the Institute regarding these two categories are briefly introduced.

1. INTRODUCTION

It is an obvious truism that, structures should be constructed on good quality ground. The ground conditions of construction sites throughout the world, however, have become worse than ever during recent decades. Often soft soils are encountered when any type of infrastructure is constructed. Large ground settlement and stability failure can be anticipated from these soft soils. Apart from clayey or highly organic soils, loose sand deposits under a water table can also cause the serious phenomena of liquefaction under seismic conditions. In these cases, suitable soil improvement techniques are required in order to improve physical and mechanical properties of the soft soil to cope with these problems. There are many soil improvement techniques developed for these purposes.

Many numerical analyses and physical model tests have been conducted to investigate the ground behavior, interactions between original ground, improved ground and superstructures, and the performance of improved ground. Based on these research results along with observations and experiences in the field, design procedures for ground improvement techniques have been established and improved.

The behavior of improved ground is affected by many factors such as the properties of the original ground and the improved ground, interactions between the original and the improved ground, external loading conditions, *etc*. In addition, the properties of original, unimproved ground after improvement are not the same as those before improvement. This is because the original ground is subjected to disturbance and stress due to the execution of ground improvement in many cases (the smear phenomenon in the vertical drain method is a typical example).

Many centrifuge model tests have been carried out as research on the topic of ground improvement. These can be classified into two categories: the investigation of soil properties' changes and the behavior of original ground during ground improvement work or the investigation of the behavior of improved ground. For the first, miniature ground improvement machines were developed to simulate actual ground improvement work in centrifuge as precisely as possible. The installation of sand drains, the heavy tamping method by Mikasa *et al*. (1989), the sand compaction pile method by Ng *et al*. (1998) and by Weber *et al*. (2006) are typical examples of this category. Centrifuge modeling of ground heaving due to the installation of compacted sand piles can be also included in this category. In the latter, the Port and Airport Research Institute carried out a large number of model tests for various ground improvement techniques. As the behavior of improved ground is affected by many factors, idealization or simplification of the problem is inevitable in centrifuge modeling and different materials and improvement processes than actual conditions were adopted in many tests.

The Soil Stabilization Laboratory of the Port and Airport Research Institute, where the authors work/worked at, carried out many centrifuge model tests over many years on research topics relating to several ground improvement techniques (Kitazume, 2009). In this paper, several examples of centrifuge modeling from the two categories previously mentioned are introduced. These were carried out in the centrifuge of the Institute (Kitazume and Miyajima, 1995).

2. INSTALLATION OF COMPACTION GROUTING

2.1 Introduction

Compaction grouting, an in-situ static compaction technique carried out by means of grout injection, has been in use since the 1960's in the United States for settlement control and bearing capacity improvement. It has been increasingly adopted in recent years for improving the liquefaction resistance of loose sandy ground (Coastal Development Institute of Technology, 2007). An increase in the liquefaction resistance of sand by compaction grouting is presumed to be derived from three possible mechanisms. They are: (i) an increase in the lateral confining stress, (ii) densification, and (iii) reinforcement by hydrated and hardened grout piles. A design of grouting specifications should, in theory, be based on these mechanics. In practice, however, most existing designs are done with a rule-of-thumb approach. The above factors are only evaluated with SPT-*N* values before and after execution. A case for the latter approach in Japan is the accumulated data and confidence from the sand compaction pile method in the past. However, this practice, being highly empirical in nature, cannot be blindly extrapolated to conditions that are outside of past experience.

Detailed, systematic studies of ground condition changes due to compaction grouting have been limited in number. The study by Nichols and Goodings (2000) is one of the few reported cases in which compaction grouting was simulated in a centrifuge. Other researchers mostly performed 1-*G* miniature model tests in calibration chambers (e.g. Shinsaka *et al*., 2003; Yamazaki *et al*., 2008; El-Kelesh and Matsui, 2008). While the above studies were helpful in drawing an outline of ground behavior during compaction grouting, they typically focused on a single grout pile installation and offer little insight into the state of ground with multiple piles. Understanding the process of stress change for progressive, multiple grout pile formation is a necessary step to move from a basic study to a practical, quantitative study of the stabilization effects.

In-flight apparatus capable of injecting three grout piles continuously was developed to investigate the stress changes caused by multiple grout piles' installation. A complete description of the study is given by Nishimura *et al*. (2011), and this chapter provides a concise summary of the adopted techniques and major findings.

2.2 Experimental setup

2.2.1 Grout injection system

The assembly used is shown in Figures 1 and 2. The soil container used is cylindrical, with an inner diameter of 540 mm and a depth of 500 mm. It has a rigid steel wall, whose inner side was lubricated with silicone grease and a layer of latex membrane. The steel wall was reinforced by welded vertical ribs to bear the load from the hoist system above it. The hoist system consists of a steel frame carrying three linear-head motors diametrically deployed 120^o apart from each other. Each of them is driven independently, lifting three rams, each of which holds an injection rod. The horizontal locations of the rods are adjustable in the radial direction allowing the rod spacing to be changed with the triangle center fixed at the container center. The motor gears were set to a lift rate of 1.1 mm/sec. Quantities presented here are in the model scale, and they are related to the proto-type scale quantities via similitude factors shown in Table 1.

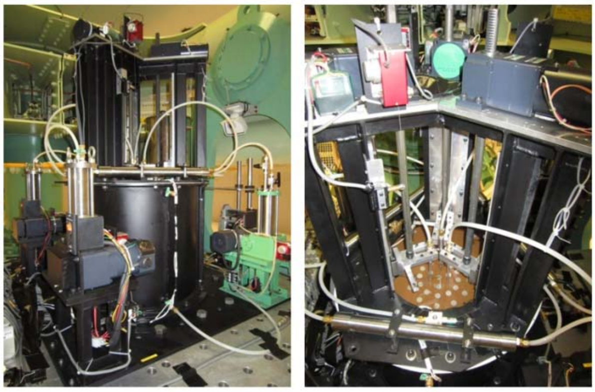

Figure 1 View of centrifuge platform after apparatus setup

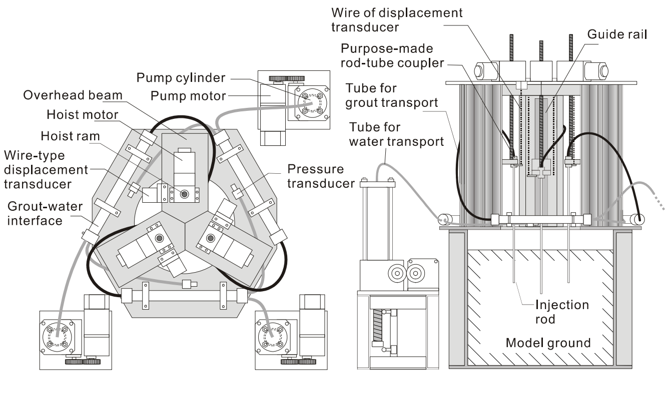

(a) Plane view (b) Vertical cross-section

Figure 2 Illustration of soil container and grout injection system

Table 1 Comparison of grout injection specifications between model and prototype
(factors with *n* indicate scale ratios of prototype to model)

Acceleration (G)	Equivalent pile diameter, d (mm)	Bulb volume (l)	Injection rate (l/min.)	Vertical injection step (mm)	Time for injection per bulb (sec.)
(n)	(1/n)	(1/n^3)	(1/n^2)	(1/n)	(1/n)
1	700	128	20.7*	333	371
30	23.3	0.00475	0.0230	11.1	12.4

*Upper bound to commonly adopted rates in Japan is 30 l/min. (CDIT, 2007)

Three motor-driven hydraulic pumps were also mounted beside the container on the centrifuge. The pumps have a pressure capacity of more than 10 MN/m^2 and the injection rate can be preset at any value between 0 and 0.4 ml/sec. The injected volume was calculated by monitoring the piston displacement. The pumps were filled with water to generate water pressure, which was then applied to the grout stored in the interface cylinders mounted on the soil container rim. Each interface cylinder had a smooth piston inside to transfer force with a minimum loss of pressure. The grout's consolidation and separation before injection, caused by self-weight under centrifugal acceleration, was mitigated by designing the cylinders in a slender shape and laying them horizontally. The injection pressure from each interface cylinder was measured by the pressure transducer connected to the cylinder's water chamber.

The grout displaced from the interface cylinders was sent to the injection rods. These were made of stainless steel, with inner and outer diameters of 5 and 8 mm, respectively, and a length of 45 mm. Thick and stiff Synflex tubes were used for water and grout transport between the pumps and the cylinders, as well as between the cylinders and the rods. The connection of the tubes was made with couplers produced by Swagelok Company, which have a straight, smooth inner wall with the same diameter as that of the Synflex tubes and the injection rods. This arrangement ensured that the grout's passage diameter was constant, reducing the possibility of clogging. It was also essential to put a small amount of high-viscosity silicone grease ahead of the grout's advancing front. This prevents free-fall of grout from the highest point in the tube under centrifugal acceleration at the initial stage of injection. Such free-fall leads to instant separation of the grout, with the separated sand particles jamming the rod tip.

2.2.2 Grout preparation

The mortar grout used in the compaction grouting technique is normally prepared by mixing a few different kinds of soil to adjust the gradation. This is so that the grout is sufficiently fine to flow through the tube and rod, while sufficiently coarse to displace the original ground without infiltrating voids. To simulate a grouting process in the miniaturized centrifuge model, consideration must be given for the small tube and rod inner diameter. Through trial and error of mixing and injection, the present study found a suitable mixture: Soma Silica Sand #5, Kawasaki Clay, Portland cement and water at ratios of 40, 60, 12, and 50% by weight. A small dose of retardant (7% of the cement weight) was admixed to prevent the early hydration of cement before injection.

2.2.3 Ground model and grout injection procedures

A typical ground model is illustrated in Figure 3 by horizontal and vertical cross-sections. The ground was prepared by air-pluviation of Soma Silica Sand #5, with a target relative density, D_r, of around 60%. Most of the test cases involved dry sand ground, while some tests were performed with sand ground saturated with viscosity-adjusted fluid. The grout pile spacing, x, was set at 1.8, 2.4, or 3.0 m with a fixed equivalent pile diameter, d, of 0.7 m (quantities are quoted in the prototype scale hereafter). The improvement ratio, a_s, is defined as the pile's horizontal cross-section area per ground area and then varied according to x. The in-practice spacing used so far in Japan has been 2.0 m or less, with a corresponding improvement ratio of 5% or more.

Grout pile installation was conducted in a bottom-up sequence once the ground model was subjected to a centrifugal acceleration of 30G The subsequent procedures involve alternating stages of injection and rod-lifting, starting from a depth of 9.9 m up to 2.4 m, in 0.33 m steps. The specifications of the injection are summarized in Table 1, which also indicates the model-to-prototype conversion ratios. The injection and lifting rates are both specified to be compatible with those commonly adopted in practice. Once a single grout pile was formed through Rod 1, the same procedures were repeated for Rod 2 and then Rod 3. Preliminary tests with pore water pressure probes confirmed that the excess pore water pressure was negligible during testing with saturated ground models.

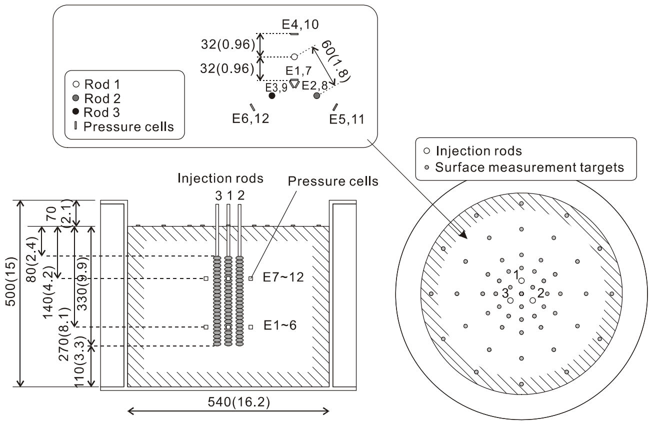

Figure 3 Example of vertical and horizontal cross-sections of ground model : Model scale in [mm] (Prototype scale in [m])

2.3 Formation of grout piles and injection pressure

The grout piles formed during the centrifuge tests were observed by excavating the ground model after the centrifuge was stopped. A typical view of the formed piles is shown in Figure 4. They resemble real grout piles formed in the field, with no obvious discontinuity or tapering trend. The equivalent pile diameter after testing, calculated from the length and the volume, was typically 0.60 to 0.63 m. The injected volume used was configured for a diameter of 0.70 m. This discrepancy was accounted for by the loss of grout water during and after injection, probably caused by radial consolidation. This consolidation might be exaggerated in the miniaturized centrifuge tests, in which the cement hydration time could not be reduced according to the similitude law. In the field, grout may start hardening before consolidation is complete, while this is unlikely in the 1/30 scale model. As this phenomenon suggests, perfect modeling satisfying simultaneous scaling of mechanical and chemical processes is difficult in many instances. Understanding and accounting for such inconsistencies is important in relating experimental findings to actual geotechnical practices.

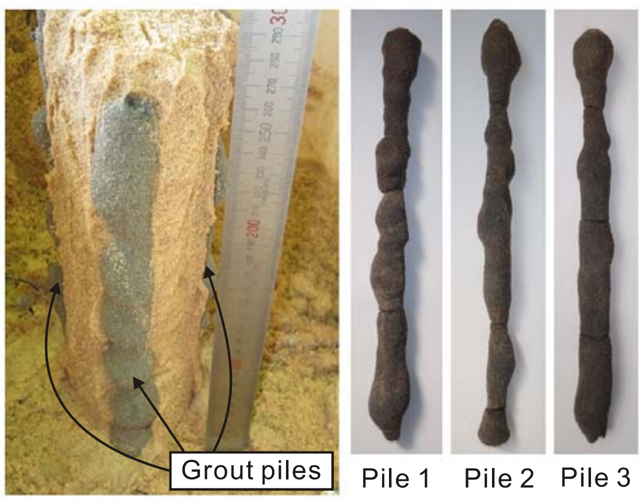

Figure 4 Grout piles formed in test case, x = 1.8 m and dry sand ground

An example of time-history of injection pressure, as measured by the pressure transducers, is shown in Figure 5. The pressure loss between the injection rod tip and the water reservoir, caused by the piston friction and grout viscosity, was calibrated and found to be a maximum of 100 kPa. This was small in relation to the pressure magnitude involved in the tests, and thus no correction has been applied to the data shown here. It is noted in the figure that the pressure reached ultimate values quickly after resuming injection. The ultimate pressure, P_u, is plotted against depth for each test case in Figure 6. It is roughly linear above 8 m depth, while later injections via Rods 2 and 3 tend to exhibit slightly higher P_u values, reflecting gradual stress build-up and an increasing degree of compaction.

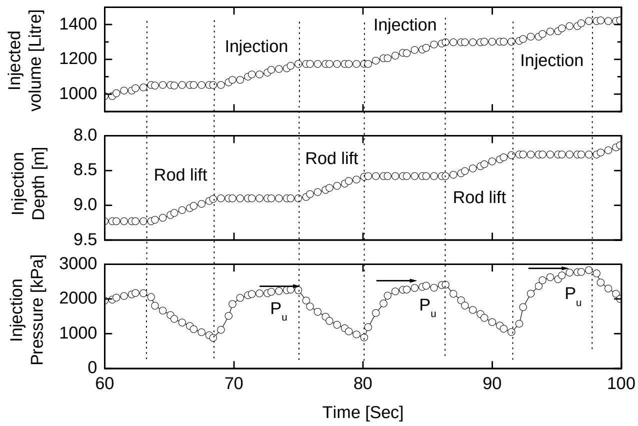

Figure 5 Time-history of injection operation and recorded injection pressure

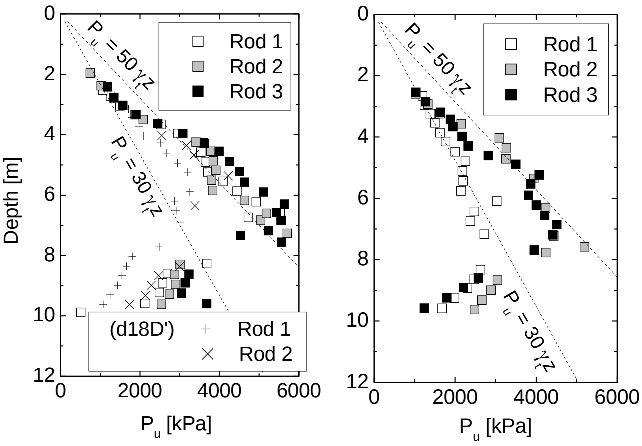

(a) x = 1.8 m (Case d18D) (b) x = 3.0 m (case d30D)

Figure 6 Ultimate injection pressure, P_u, recorded against depth (d18D', an unsuccessful case in which grout jammed in Rod 3, serves as a duplicate case of injection via Rods 1 and 2 in d18D, a dry sand case with x = 1.8 m)

The lines representing P_u=30$\gamma_t z$ and P_u=50$\gamma_t z$ (γ_t is the dry unit weight and z the depth), also shown in Figure 6, seem to bracket the experimental date. These factors, 30 - 50, are compatible with the commonly quoted field values of 20 - 100 (e.g. Shinsaka *et al*., 2003). Shinsaka *et al*. (2003) found that a factor of only 8 - 10 was obtained in their miniaturized 1-*G* model tests. It is thus suggested that reproducing the stress level found in the field is an important factor in quantitatively studying the pressure and stress characteristics involved in compaction grouting. Below 8 m in depth, the P_u values exhibited reverse, increasing-upward trends.

This P_u-z curve shape may indicate the combined effect of two mechanisms at work simultaneously. As the injection point moved upward, the previously compacted region beneath the current injection point functioned as a foundation, providing larger bearing capacity against subsequent injection, resulting in an increasing-upward trend. At the same time, the overburden pressure, which also resisted the expansion of the grout bulb, decreased in proportion to the injection depth, resulting in a decreasing-upward trend.

2.4 Summary

Apparatus and experimental techniques for simulating compaction grouting were developed and confirmed to be successful, with relatively uniform grout piles formed in the centrifuge. The recorded level of injection pressure was consistently within the range commonly encountered in field execution, suggesting that the centrifuge testing, by reproducing realistic stress levels in the ground, was an appropriate model of the problem. Following this success, this study investigated the stress state changes caused by grout injection and proposed to take into account new stress states as well as sand densification in the evaluating the effect on liquefaction resistance improvement. The details are reported by Nishimura *et al*. (2011).

3. BEARING CAPACITY OF SAND COMPACTION PILE IMPROVED GROUND

3.1 Introduction

The sand compaction pile method (SCP) has been used to improve soft grounds often found in the Japanese coastal area (Kitazume, 2005). When this method is applied to clay deposits, the improved ground is often called composite ground. The behavior of the improved ground is influenced by many factors, including geometric conditions and initial and induced stress conditions in the ground. Also the in-situ sand pile properties can be scattered, and the surrounding ground in many cases is heavily disturbed due to pile installation. There are two approaches in modeling the improved ground in centrifuges: one method similar to the in-situ technique is adopted to make a model ground having similar properties to that of the in-situ or an ideal and simple ground model is prepared to avoid any influence factors due to uncertainties in field conditions. The authors adopted the second approach in which frozen sand piles were prepared separately and installed into holes in the model ground to avoid the influence of soil disturbance due to pile installation. Here one such study is reported, investigating the bearing capacity of the SCP improved ground with a low improvement area ratio, a_s under a combination of vertical and horizontal loads (Terashi *et al*., 1991).

3.2 Preparation of model ground

The setup of the ground model is shown in Figure 7. A thick, normally consolidated clay layer of Kaolin is reduced in scale and prepared in a strong specimen box with inside dimensions: 30 cm deep, 10 cm wide, and 50 cm long. All the model tests were carried out in the 50 *G* field. Therefore the prototype simulated in the strong box was an approximately 10 m thick alluvial clay deposit which was improved by large compacted sand piles with 1 m diameter. The material used for the sand pile and sand mound was Toyoura sand and the clay used was Kaolin clay. Both materials were selected because their characteristics are well known and also are commercially available.

A thick, normally consolidated clay layer was prepared in a strong specimen box with inner dimensions of 30 cm depth, 10 cm width and 50 cm length. The kaolin clay was thoroughly remolded at a water content of 120%, which was significantly higher than its liquid limit. A 5 cm thick drainage layer of Toyoura sand was placed at the bottom of the strong box. Then the slurry of Kaolin clay was poured into the box. Then preliminary consolidation was conducted with a vertical pressure of 10 kN/m^2 on the laboratory floor. Then the model ground was brought onto the swing platform for self-weight consolidation under 50 *G* in order to prepare a normally consolidated clay layer with a thickness of 20 cm. Due to the pre-consolidation and the self-weight consolidation, the completed model ground had a thin layer of over-consolidated clay underlain by the thick, normally consolidated clay. After the self-weight consolidation was completed, the centrifuge was stopped for the preparation of the improved ground on the laboratory floor. Model compacted sand piles were manufactured following the procedure devised by Kimura *et al*. (1982) and installed into the model ground. Saturated Toyoura sand was poured into water-filled tubes whose inner diameter was 20 mm. The sand and tubes were subjected to vibration until the specified density of the sand was attained. The prepared sand piles were then slowly frozen and both ends were then trimmed. Thin-walled tubes with 20 mm outer diameters were inserted into the clay ground in a regular rectangular pattern at a spacing of 33 mm (model scale), which corresponded to a low a_s of 0.28. Then the clay inside the tubes was removed by a tiny auger to make holes. Finally the frozen sand piles were inserted into the holes and left to thaw gradually. This procedure is different from actual practice but was adopted in the model ground preparation in order to avoid any soil disturbance due to actual pile installation. After the soil improvement, the strong box was mounted again onto the swing platform of the centrifuge for the loading test. In order to reflect the prototype loading condition of breakwaters or revetments in the model test, it was deemed most appropriate to apply the vertical load component in advance to applying the horizontal load component. The vertical load component was applied by a quick lowering of the water level. The horizontal component was applied immediately after that by means of the horizontal loading jack.

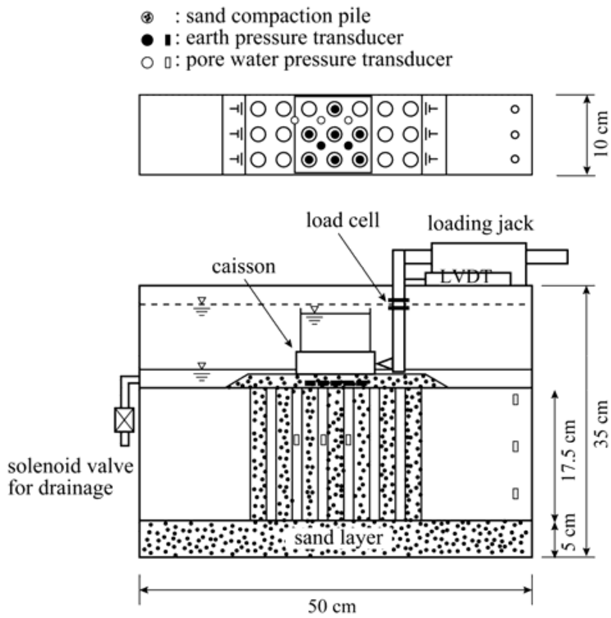

Figure 7 Setup of the model ground (model scale)

3.3 Test results and discussion

During the vertical loading test, the load increased with increasing settlement and neither peaking nor a final constant load was observed. The bearing capacity of the improved ground was determined as the yield of the ground. The yield load of the ground was defined as the intersection of the initial tangent line of the curve and the tangent line at the straight portion of the curve with the larger settlement.

For the inclined load tests (see Figure 10 for the load inclination in each test), horizontal load, *H* versus horizontal displacement, δ_h curves are obtained and shown in Figure 8. In test No. 3 for the largest load inclination, the *H* increases with increasing δ_h but the load becomes constant after reaching a certain value. The bearing capacity for this particular case is therefore determined as this final constant value. However, the *H* - δ_h curves for smaller load inclinations do not show either peaking or a final constant value. The bearing capacities for these cases are determined by the intersection of two tangent lines, as shown by the arrows in the figure. As shown in the figure, it is seen that the horizontal component of the bearing capacity is highly dependent upon the load inclination.

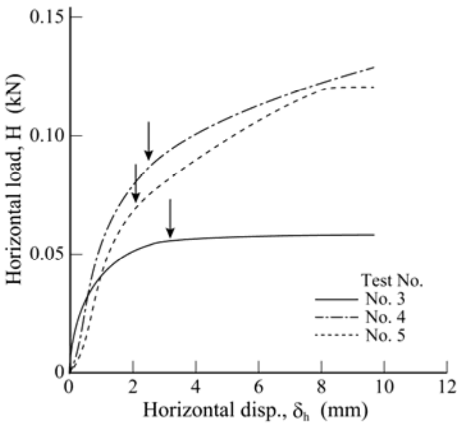

Figure 8 Horizontal load - displacement curves

Figure 9 shows the photograph taken after the vertical load test (Test No. 1) to observe the deformation of sand piles directly. Shear planes and a sliding wedge are clearly observed in the central three rows of sand piles. The piles outside the wedge are deformed at their tops by the penetration of wedge but the overall improved ground does not reach general shear failure.

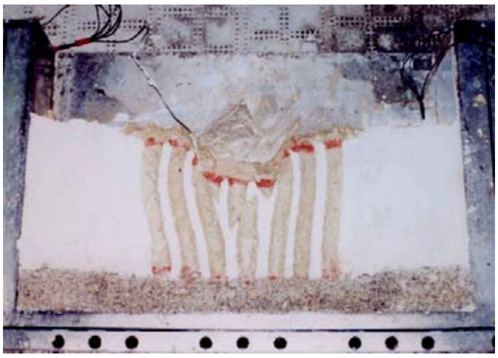

Figure 9 Failure mode of compacted sand piles (No.1)

The vertical and horizontal load components, *V* and *H* at yield or failure of the improved ground for all the tests are plotted in Figure 10 to obtain the bearing capacity envelope on the *V* - *H* plane. The horizontal load which can be supported by the improved ground increases with increasing vertical load. However, when the *V* reaches about half of the vertical bearing capacity, the *H* reaches a maximum and decreases with a further increase in *V* .

Several failure criteria for the composite ground have been proposed and employed in routine design for many years in Japan. Bearing capacity is calculated by the Fellenius method of slip circle analysis combined with a shear strength expression and shown by a solid curve in Figure 10. The curve produces a cigar-shaped bearing capacity envelope in the *V* - *H* plane and is acceptable both qualitatively and quantitatively. Also calculated and shown by a solid straight line in Figure 10 is the simple sliding failure of the foundation on the surface of sand mound. For this failure mode, the maximum horizontal load is calculated as a product of the effective weight of the foundation and the factor of friction of the sand mound. As is observed in the figure, the results obtained both by calculation and experiment are in accordance with sliding failure.

3.4 Summary

These test results were employed in the development of design formula for improved ground by the sand compaction pile method with low replacement area ratio. The centrifuge test results corroborated the analytical prediction of the improved ground's bearing capacity under combined loads, thus adding confidence to the predictive method.

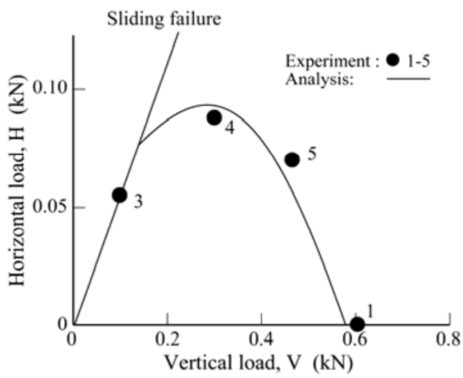

Figure 10 Bearing capacity envelope in the *V* - *H* Plane

4. STABILITY OF GROUP COLUMN DEEP MIXING TYPE IMPROVED GROUND

4.1 Introduction

The Deep Mixing Method, a deep, in-situ soil stabilization technique using cement and/or lime as a binder was invented and developed by the Port and Harbour Research Institute (PHRI; the former body of PARI) to improve soft marine deposits (Coastal Development Institute of Technology, 2002; Kitazume and Terashi, 2013). Providing a quick strength increase and high shear strength for stabilized soil, DMM has become one of the most effective soil improvement techniques for marine and on-land constructions. Group column type improvement, where many columns are constructed in rows with rectangular or triangular arrangements, has been extensively applied to foundations of embankments or lightweight structures. Design procedures for improved ground have been established in Japan, in which two failure patterns are assumed: external and internal instabilities as shown in Figure 11 (Public Work Research Center, 2004). For external failure, the possibility of sliding failure is calculated, in which the DM columns and the clay between move horizontally in a stiff layer without any rearrangement of columns (i.e. a failure mechanism occurs outside the improved region). In the internal stability analysis, rupture breaking failure is calculated with slip circle analysis, in which the shear failure mode of DM columns is assumed (i.e. a failure mechanism occurs within the improved region).

The first author investigated the failure mechanism and stability of group column type improved grounds subjected to embankment loading (Kitazume and Maruyama, 2006; 2007). In the centrifuge modelling of external failure, acrylic pipes were used as model stabilized soil columns instead of a mixture of soil and cement, in order to measure the axial force and bending moment induced in the pipes. For internal stability testing, a mixture of soil and cement was used as model soil columns to simulate its failure in the centrifuge. In both cases, an ideal and simple model ground technique was adopted to avoid any influence due to the columns installation. The model columns prepared separately were installed into holes in the ground. In this section, the test results on the failure pattern of the improved ground and the criteria related to external and internal stabilities are briefly introduced.

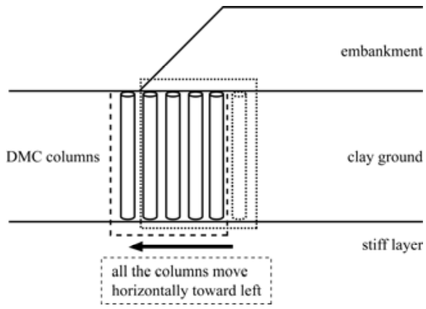

(a) External instability (sliding failure)

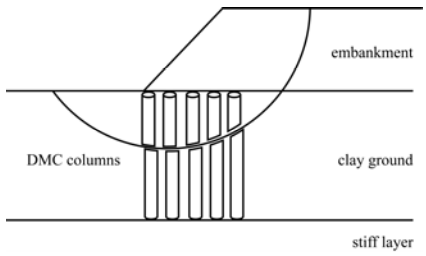

(b) Internal instability (rupture breaking failure)

Figure 11 Assumed failure patterns of DM improved ground in the current design method

4.2 Preparation of model ground

Figure 12 schematically shows a typical example of model ground setup, in which a 20 cm thick normally consolidated clay ground of and five rows of DM columns are modeled. In the model ground preparation, a drainage layer of Toyoura sand was made on the bottom of the specimen box. Kaolin clay slurry was poured on top of the layer and then pre-consolidated one-dimensionally with a vertical pressure of 9.8 kN/m^2 on the laboratory floor. After self-weight consolidation was completed at 50 *G*, the centrifuge was stopped for the preparation of the improved ground on the laboratory floor. A thin-walled tube with an outer diameter of 20 mm was penetrated into the clay ground. The clay inside the tube was then carefully removed using a tiny auger, and a model DM column was inserted after removing the tube. Similar to the SCP model ground preparation, this procedure is different from actual practice but was adopted in order to avoid any soil disturbance due to the actual method of constructing stabilized soil columns.

4.3 Test procedure

The model ground was then brought up to a 50 *G* centrifugal acceleration field, which corresponds to a 10 m thick soft clay layer improved by DM columns of 1 m diameter in a prototype scale. The model ground was allowed to consolidate again by the enhanced self-weight to minimize any soil disturbance that might be induced during the model ground preparation. After consolidation, the model embankment was constructed stepwise under almost undrained conditions by the in-flight sand raining device.

In the test series, two types of model column, an acrylic pipe and cement stabilized columns, were used as a DM column. The both columns have 2 cm in diameter and 20 cm in length. A total of 11 model tests were carried out as summarized in Table 2. Acrylic columns (named as A-column) were used to simulate soil columns with very high strengths in Cases 2 to 5 in order to investigate the external stability with bending moment measurements. The cement stabilized columns (named as Tl-column and Th-column) were used in Cases 6 to 11 to investigate the internal stability while simulating rupture breaking failure. In order to detect the model column failure during loading, a carbon rod electric probe was embedded into the columns before hardening which are placed in rows b, c and d, marked by red circles in Figure 12 (Kitazume and Maruyama, 2007).

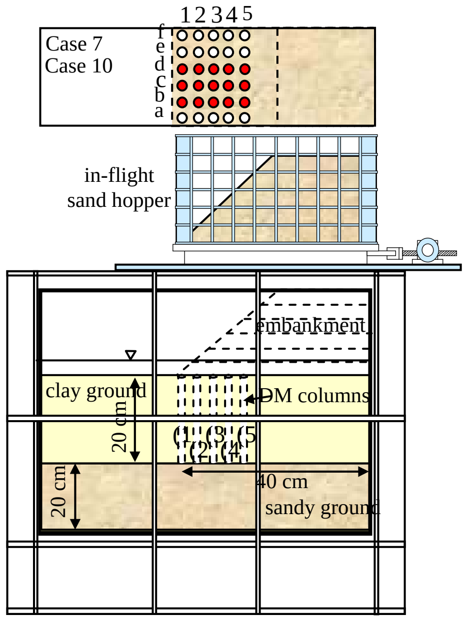

Figure 12 Model ground setup (Cases 7 and 10)

Table 2 Test conditions and major test results

	Improvement condition				
	Width (cm)	No. of rows	Imp. area ratio, a_s	material	q_u (kN/m^2)
Case 1	0	-	-	-	-
Case 2	8.6	3	0.28	A	-
Case 3	15.2	5	0.28	A	-
Case 4	21.8	7	0.28	A	-
Case 5	15.2	5	0.56	A	-
Case 6	8.6	3	0.28	Tl	425
Case 7	15.2	5	0.28	Tl	411
Case 8	21.8	7	0.28	Tl	391
Case 9	8.6	3	0.28	Th	1271
Case 10	15.2	5	0.28	Th	1290
Case 11	21.8	7	0.28	Th	1434

4.4 Test results and discussion

The measured embankment pressure and displacement curves for the external stability study (Cases 1 to 4) are shown in Figure 13(a). In the figure, the vertical and horizontal axes show the embankment pressure, p_e, measured at the ground surface and the horizontal displacement at the toe of embankment slope, δ_h, respectively. In the unimproved ground (Case 1), a relatively small horizontal displacement takes place as long as the embankment pressure remains at a very low level, but the displacement increases rapidly with a further increase of embankment pressure. On the other hand, in the improved ground with A-columns (Cases 2 to 4), the horizontal displacement increases with increasing embankment pressure, but its magnitude is small compared to that in the unimproved ground. The magnitude of horizontal displacement becomes smaller as the improvement width increases.

The p_e and δ_h curves of Cases 7 and 10 for internal stability are plotted in Figure 13(b). In the figure, the letters beside the curves indicate column ruptures, indicated by the ID number of the columns as shown in Figure 12. In Case 7, the Tl-1b column failed first at a p_e of 26.2 kN/m^2, and Tl-2b, Tl-2d, and Tl-3c all failed at the same time. As p_e increased, the columns failed one by one in sequence from the foremost to the rearmost column. In Case 10, the foremost columns failed one by one at a p_e of 34.2 to 50.2 kN/m^2. When p_e increased to 79.6 kN/m^2, Th-5b, Th-5c, and Th-5d failed instead of the second, third, and fourth row columns. After that, Th-4 and Th-3 failed in reverse sequence from the rearmost to the foremost column. It is interesting to note that p_e continually increased even after many columns failed.

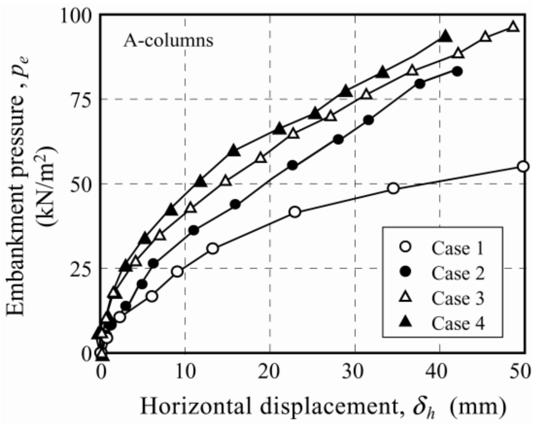

(a) for external stability study (Cases 1 to 4)

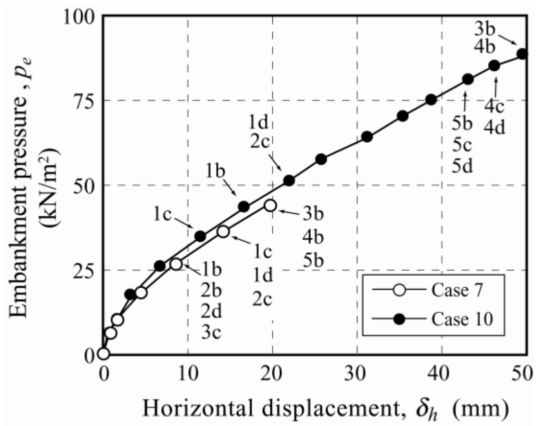

(b) for internal stability study (Cases 7 and 10)

Figure 13 Embankment pressure and horizontal displacement curves

The DM columns after embankment loading in Cases 3, 7, and 10 are shown in Figure 14. In Case 3, Figure 14(a), all the columns tilted like dominos about their toe without any breaking failure. The inclination angle was the same for all the columns, indicating that the improved area deformed uniformly as a simple shear failure. This failure pattern is quite different from that in the external stability analysis of the current design method where the sliding failure pattern is assumed.

In Case 7, Figure 14(b), all the columns titled counterclockwise with bending failure. As the embankment loading was terminated at a relatively small embankment pressure to prevent heavy column failure, the tensile cracks cannot be observed clearly in the figure. According to Figure 13(b), Tl-1b and Tl-2b failed first and then the other three columns (Tl-3b, Tl-4b, and Tl-5b) failed at the same p_e of 43.9 kN/m^2. In Case 10, Figure 14(c), the columns tilted counter-clockwise with tensile cracks at two depths. The figure clearly shows that the column did not fail by shear failure but rather by bending failure. According to the detailed observation after the test, the bending failure took place at a shallow depth first and then at a deeper depth.

According to the failure pattern observed in the model tests, a simple stability calculation was carried out. For the calculation of the external stability of clay ground the columns were assumed to deform as a result of simple shearing due to the unbalanced pressure of active and passive earth pressures acting on the side boundaries of the improved area. For the calculation of the collapse failure pattern, the moment equilibrium at the bottom of improved area was

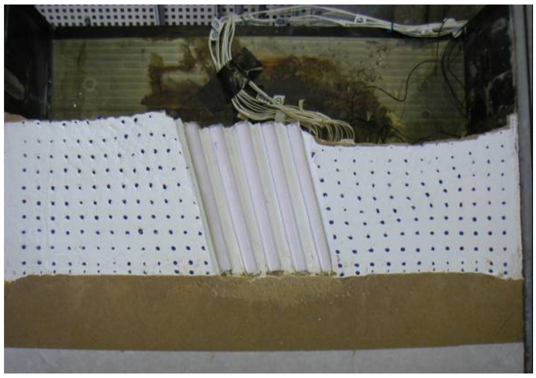

(a) Case 3

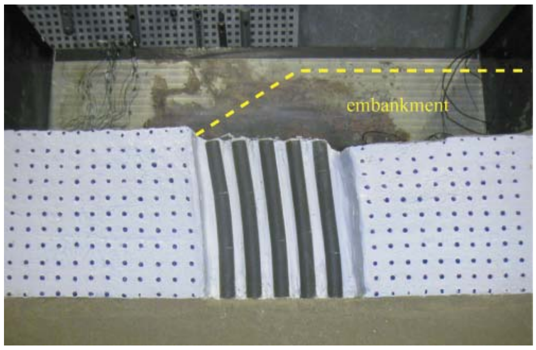

(b) Case 7 (b-line)

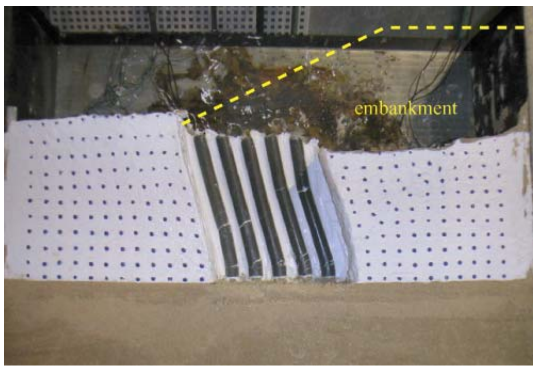

(c) Case 10 (c-line)

Figure 14 Failure pattern of improved ground analyzed. The calculated $p_{ef,collapse}$ for various stress concentration ratios, *n,* and friction angle of embankment, ϕ_e, are plotted in Figure 15 against the improvement width, *D*. The $p_{ef,collapse}$ increases almost linearly with *D* for all cases. The effects of ϕ_e and *n* are quite small on $p_{ef,collapse}$ and the *n* value in particular has a negligible effect. In the figure, the model test results are also plotted. Although the calculated $p_{ef,collapse}$ still overestimates the test results for small *D* for large *D* the data is well correlated. The calculation provides reasonable estimations compared with the experiments.

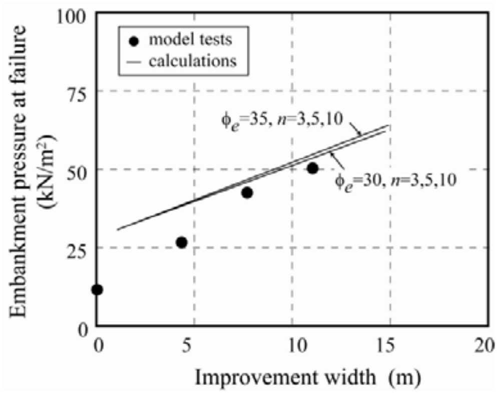

Figure 15 Relationship between improvement width and embankment pressure at ground failure

A series of calculations was carried out for various widths and column strengths, and the relationship between the width between columns, *D*, and the failure depth, *z*, is shown in Figure 16 for various q_u values. It is found that *z* increases monotonically with increasing *D* and with increasing q_u. However, the effect of q_u is not so dominant as compared to the shear failure pattern. In the figure the model test results are also plotted. The calculation gives a reasonable estimation of the failure depth, in which the calculations slightly overestimate the model test results for Cases 6 to 8 but underestimate for Cases 9 to 11.

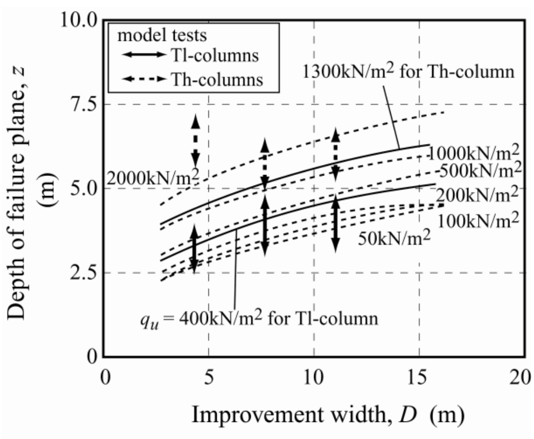

Figure 16 Relationship between the improvement width and the failure depth for bending failure mode

For internal stability, a simple stability calculation was also proposed. In the calculation, all the DM columns were assumed to fail simultaneously with the bending failure mode and the improved area above a failure plane was assumed to deform as simple shearing. For the calculation, the moment equilibrium at the assumed failure plane was formulated. The $p_{ef,bending}$ is shown against *D* in Figure 17.

The figure shows the $p_{ef,bending}$ value increases with increasing *D* and q_u. However, the effect of q_u is relatively small. The model test results are also plotted in the figure. Comparing them, the calculations give a reasonable estimation to the model tests.

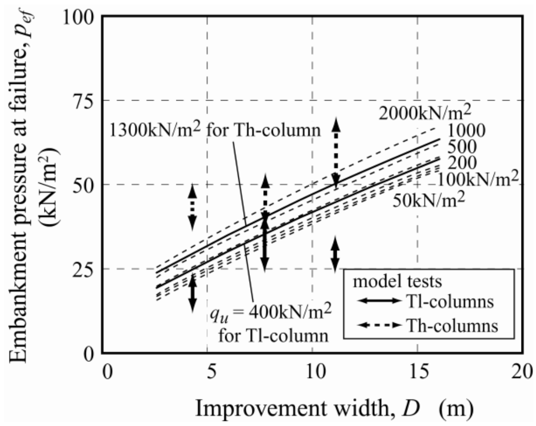

Figure 17 Relationship between improvement width and embankment pressure at ground failure

Figure 18 shows the combined failure criteria for the external and internal stabilities plotted against various column strengths. The figure clearly shows that the criteria for the internal stability gives a low embankment pressure when the column strength is lower than 1000 kN/m^2 or the improvement width is smaller than about 12 m. This indicates that the breaking failure of DM columns takes place first instead of the collapse failure of the ground. In the case where the column strength exceeds about 2000 kN/m^2 and the improvement width exceeds about 12 m, the external stability gives lower pressure than the internal stability. This means that the collapse failure of the ground takes place before the breaking failure of DM columns.

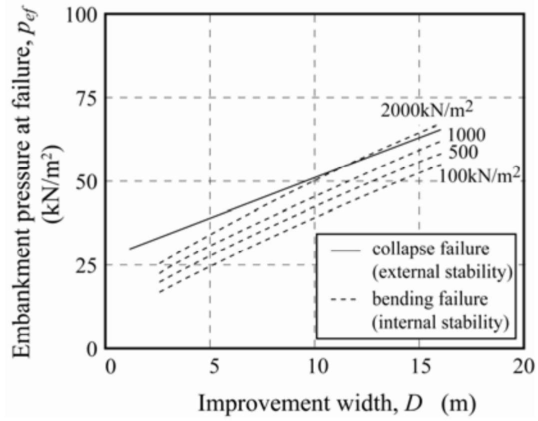

Figure 18 Failure criteria of external and internal stability of group column DM improved ground

4.5 Summary

According to the tests, it is found that the current design method overestimates the model test results in the external and internal stabilities, because inadequate failure patterns are assumed in the analyses. The proposed calculations based on the centrifuge model tests have relatively high applicability for evaluating the external and internal stability of the group column DM improved ground.

5. EFFECT OF DEEP MIXING WALL SPACING ON LIQUEFACTION MITIGATION

5.1 Introduction

The deep mixing method has been adopted for many construction projects for improving stability and reducing settlement of soils. Recently, grid type improved ground has also been applied for liquefaction prevention, in which a grid of stabilized columns functions to restrict generation of excess pore pressure by confining the soil particle movement during an earthquake. The improvement effect of the technique was confirmed in the 1995 Kobe earthquake (Tokimatsu *et al*., 1996). Experimental and numerical studies have been carried out to investigate the effect of grid spacing on pore pressure generation and liquefaction prevention (e.g. Namikawa *et al*., 2007). Based on these studies, a quite simple guideline for the method was established. However, the current design practice of this method does not take into account different seismic behavior that occurs at different depths but evaluates the possibility of liquefaction only at the middle depth.

A series of centrifuge model tests was conducted to investigate the effect of grid spacing on generation of pore pressure and seismic response in a sand layer. In this research, the spacing of grid is the main concern and the failure of the wall is not priority. Therefore the model wall was prepared by Bakelite material instead of the mixture of soil and cement. The effect of grid spacing was assessed in the other centrifuge tests by taking into account the ratio of grid spacing to depth (Takahashi *et al*., 2006).

5.2 Preparation of model ground

An example of model grounds is schematically shown in Figure 19, where two model grounds with different sizes were prepared in a specimen box for conducting many tests. The model grid was made of Bakelite panels with a thickness of 2 cm, as shown in Figure 20. The model grid was fixed on the specimen box with bolts. Several model grids were prepared to perform parametric tests.

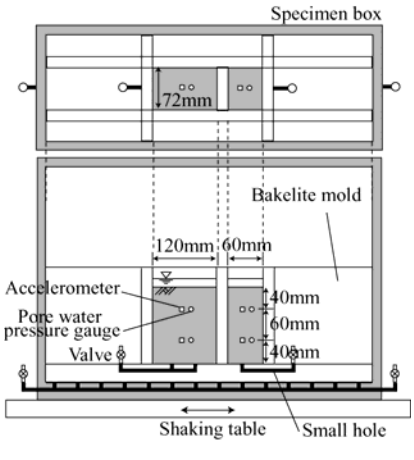

Figure 19 Schematic view of model ground

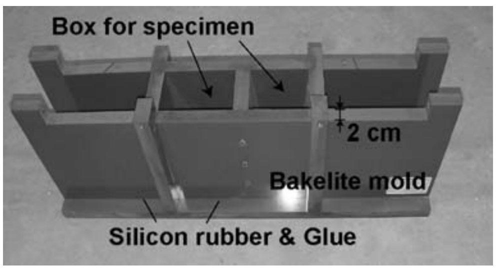

Figure 20 Bakelite panels

The sand used in this study was Soma sand, whose U_c and D_{10} are 1.7 and 0.34 mm respectively (Takahashi *el al*., 2006). Several accelerometers and pore pressure gauges were placed precisely at a depth of 4 cm and 10 cm from the ground surface. After filling the sand, the ground surface was carefully leveled by means of a vacuum, and then fully saturated by the percolation technique using Carbon dioxide gas and a vacuum. The fluid used in this study was an aqueous solution of hydroxypropyl methylcellulose. The viscosity of fluid was controlled to be 25 m^2/s for the 25 *G* centrifuge model test by changing its concentration.

5.3 Test procedure

Soon after reaching a centrifugal acceleration of 25 *G*, the model ground was subjected to seismic excitation of 50 sinusoidal waves at 4 Hz in the prototype scale. After confirming the dissipation of excess pore pressure generated in the previous excitation, the excitation level was increased stepwise until the model ground liquefied. A total of eleven model tests were carried out on the model ground prepared with various types of grid spacing, as summarized in Table 3.

Table 3 Test conditions

Case	Wall spacing, *L* (m)	Relative density (%)	Viscosity (m^2/s)
E1-1	1.5	49.7	23.6
E1-2	1.5	44.0	15.2
E2-1	2.0	44.0	21.5
E2-2	2.0	41.7	13.0
E3-1	2.5	44.0	21.5
E3-2	2.5	41.7	13.0
E4-1	3.0	49.7	23.6
E4-2	3.0	44.0	15.2
M25-5	6.0	33.7	18.3
M25-6	6.0	53.0	20.9
M25-7	6.0	50.0	24.2

5.4 Test results and discussion

The relationship between the induced acceleration at a depth of 1.0 m (values are quoted in prototype scale in this subsection) and input excitation are plotted in Figure 21. The induced acceleration measured in various grid spacing initially increases almost linearly with increasing input acceleration. The induced acceleration for the wall spacing *L* equals 2.0 m, shows a sharp decrease at an input excitation of about 380 gal, which indicates that liquefaction took place in the ground. The model ground with an *L* of 1.5 m does not show a sharp decrease in acceleration even if the input acceleration exceeds about 500 gal. Similar phenomenon can be seen in the measurements at a depth of 2.5 m. The relationship between the maximum excess pore pressure ratio, $\Delta u/\sigma'$ measured at a depth of 1.0 m and the input excitation is shown in Figure 22. As the input excitation increases, $\Delta u/\sigma'$ increases gradually irrespective of the grid spacing. $\Delta u/\sigma'$ increases to unity in the case where *L* is equal to or exceeds 2.0 m, and the input acceleration at that time decreases as the *L* value increases. In ground with an *L* of 1.5 m, $\Delta u/\sigma'$ does not increase to unity even when the input acceleration exceeds about 500 gal. According to the discussion above, the improvement effect on liquefaction prevention is highly influenced by the grid spacing. Figure 23 shows the relationship between the ratio of grid spacing to the grid depth, *L/d*, and the input acceleration. The *d* is the concerned depth measured from the ground surface. In the figure, the test data when liquefaction did or did not take place is plotted as a filled circle and an open circle, respectively. A gray-filled circle shows the excitation level where the ground liquefies to some extents during the excitation. Based on the plotted data, a liquefaction boundary can be drawn as the hatched portion in the figure. The boundary shows that the input acceleration necessary for

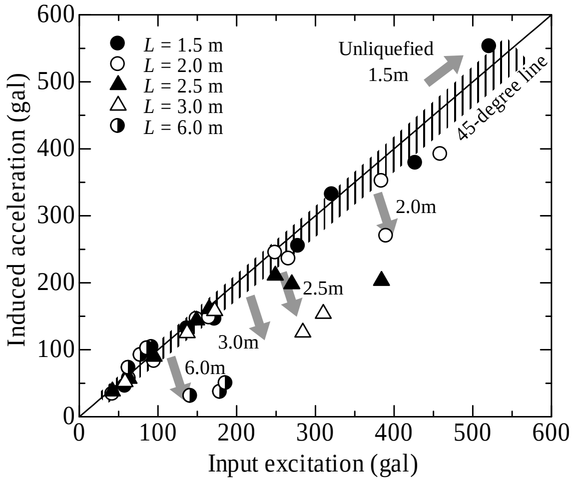

Figure 21 Relationship between induced acceleration and input excitation at a depth of 1.0 m

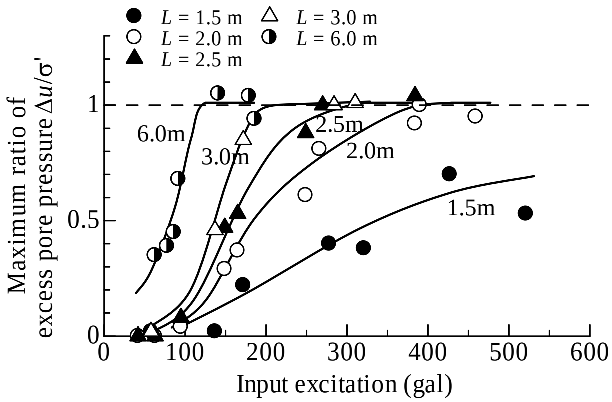

Figure 22 Relationship between maximum ratio of excess pore pressure and input excitation at a depth of 1.0 m

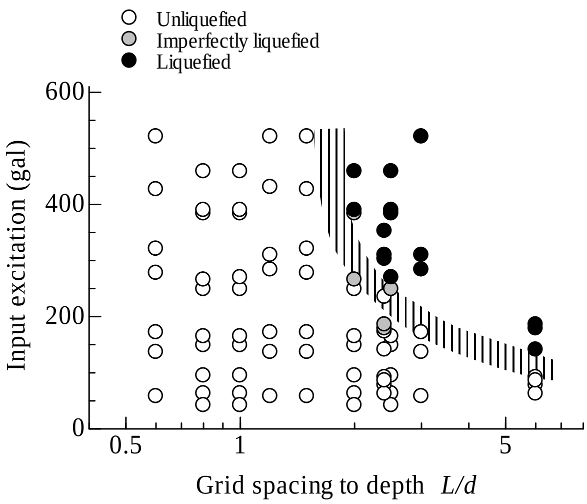

Figure 23 Relationship between input excitation and *L/d*

liquefaction increases with decreasing *L/d*, increasing very sharply when *L/d* becomes less than about 2. This figure confirms that a large effect on liquefaction prevention can be expected when the *L/d* ratio becomes less than about 2. This figure also indicates that the liquefaction can be induced by a relatively small earthquake at a shallow depth of ground (i.e. having a small *d* value) even if the grid spacing is quite small. This suggests a limitation in the application of the grid type improvement for liquefaction prevention, and that shallow ground should be improved by the other technique.

5.5 Summary

Based on the accelerations and pore pressures measured in the model ground with five different grid spacing, it was confirmed that the improvement effect of liquefaction prevention was influenced by not only the grid spacing but also the magnitude of excitation, as well as differing with depth. In the present study, a new parameter, the ratio of grid spacing to depth, *L/d*, was proposed to evaluate the effect of grid improvement on liquefaction prevention.

6. CONCLUDING REMARKS

In this paper, several examples of centrifuge modeling were briefly introduced, which included the simulation of grouting and investigations of improved ground by the sand compaction pile method and the deep mixing method. In the first, a miniature installation machine was invented to simulate the actual grouting in centrifuge as closely as possible, and the stress development during the execution was measured and studied. In the other studies, the model ground was prepared with different materials and different procedures from actual practice in order to make an idealized and simplified improved ground model as well as to avoid any effect due to the execution of improvement in the field on the behavior of improved ground in modeled testing. This approach has often been adopted in the Institute for performing parametric studies and to focus on essential issues in the behavior of improved ground. This approach requires detailed understanding and experience in the field behavior in order to apply the model test results to actual conditions. The authors also recognize alternative approaches where a model ground is prepared in similar techniques and manners to the actual as precisely as possible and apply the test results to actual situations directly. Selection of the approaches is up to the centrifuge modeler, but should be appropriately conducted considering the research target of model tests. The authors should emphasize that detailed understanding of the behavior of actual improved ground and experiences of field ground improvement work are important, irrespective of the approach.

Finally the authors wish that this paper will be useful for performing centrifuge model tests relating to ground improvement techniques.

7. REFERENCES

Coastal Development Institute of Technology (2002) The deep mixing method - principle, design and construction-, A.A. Balkema, p123.

Coastal Development Institute of Technology (2007) Technical manual of compaction grouting method as a countermeasure for liquefaction, p188, (in Japanese)

El-Kelesh, A.M. and Matsui, T. (2008) "Calibration chamber modeling of compaction grouting", Geotechnical Testing Journal, Vol.31, No.4, pp295-307.

Kimura, T., Nakase, A., Kusakabe, O., Saitoh, K. and Ohta, A. (1982) "Geotechnical centrifuge model tests at the Tokyo Institute of Technology", Technical Report No.30, Department of Civil Engineering, Tokyo Institute of Technology, pp1-33.

Kitazume, M. (2005) The sand compaction pile method, A.A. Balkema, p232.

Kitazume, M. (2009) "Twenty Nine Years of experiences of physical modeling of geotechnical problems in port structures", International Journal of Physical Modelling in Geotechnics, Vol.9, No.3, pp1-19.

Kitazume, M. and Maruyama, K. (2006) "External Stability of Group Column Type Deep Mixing Improved Ground under Embankment Loading", Soils and Foundations, Vol. 46, No. 3, pp323-340.

Kitazume, M. and Maruyama, K. (2007) "Internal Stability of Group Column Type Deep Mixing Improved Ground under Embankment Loading", Soils and Foundations, Vol. 47, No. 3, pp437-455.

Kitazume, M. and Miyajima, S. (1995) "Development of PHRI Mark II geotechnical centrifuge", Technical Note of the Report of the Port and Harbour Research Institute, No.817, p33.

Kitazume, M. and Terashi, M. (2013) The Deep Mixing Method, CRC Press, Taylor & Francis Group, 410p.

Mikasa, M., Takada, N. and Ohshima, A. (1989) "Dynamic consolidation test in centrifuge", Proceedings of the 11th International Conference on Soil Mechanics and Foundation Engineering, Vol. 2, pp947-950.

Namikawa, T., Koseki, J. and Suzuki, Y. (2007) "Finite element analysis of lattice-shaped ground improvement by cement-mixing for liquefaction mitigation," Soils and Foundations, Vol.47, No.3, pp559-576.

Ng, Y. W., Lee, F. H. and Yong, K. Y. (1998) "Development of an in-flight sand compaction piles (SCPs) installer", Proceedings of the International Conference Centrifuge 98, Vol.1, pp837-843.

Nichols, S.C. and Goodings, D.G. (2000) "Physical model testing of compaction grouting in cohesionless soil", Journal of Geotechnical and Geoenvironmental Engineering, ASCE, Vol.126, No.9, pp848-852.

Nishimura, S., Takehana, K., Morikawa, Y. and Takahashi, H. (2011) "Experimental study of stress changes due to compaction grouting", Soils and Foundations, Vol.51, No.6, pp1037-1049.

Public Works Research Center (2004) Technical manual on deep mixing method for on land works, p334 (in Japanese).

Shinsaka, T., Zen, K., Sakamoto, K. and Yamazaki, H. (2003) "Experimental studies on the compaction effect of static grouting on sand", Proceedings of the Japan Society of Civil Engineers, No.764/III-67, pp183-192 (in Japanese).

Takahashi, H., Kitazume, M., Ishibashi, S. and Yamawaki, S. (2006) "Evaluating the saturation of model ground by P-wave velocity and modeling of models for a liquefaction study", International Journal of Physical Modelling in Geotechnics, Vol.6, No.1, pp13-25.

Terashi, M., Kitazume, M. and Minagawa, S. (1991) "Bearing Capacity of Improved Ground by Sand Compaction Piles", Deep Foundation Improvements: Design, Construction, and Testing, ASTM STP 1089, Robert C. Bachus, Ed., American Society for Testing and Materials, 1990, ASTM, pp47-61.

Tokimatsu, K., Mizuno, H. and Kakurai, M. (1996) "Building damage associated with geotechnical problems", Soils and Foundations, Special Issue 1, pp219-234.

Weber, T. M., Laue, J. and Springman, S. M. (2006) "Centrifuge modelling of sand compaction piles in soft clay under embankment load", Proceedings of the 6th International Conference on Physical Modelling in Geotechnics, Hong Kong, pp603-608.

Yamazaki, H., Kaneda, K., Adachi, M., Harada, Y., Yamada, K. and Takahashi, T. (2008) "Model tests on compaction grouting method", Proceedings of the Japan Society of Civil Engineers, Series C, Vol.64, No.3, pp544-549 (in Japanese).